ZANCO Journal of Pure and Applied Sciences

TYPE Original article
DOI http://dx.doi.org/10.21271/ZJPAS.38.2.6

OPEN ACCESS

*Corresponding author
Sardar Rashid Fattah
sardar.fattah@soran.edu.iq

RECEIVED :26 /06 /2025
ACCEPTED :17/09/ 2025
PUBLISHED :30/ 04/ 2026

KEYWORDS:
Stretch-twist-fold flow system, Caputo fractional order derivative, Hopf bifurcation, Adams-type predictor-corrector approach, Lyapunov exponents.

Chaotic and Hopf Bifurcation Analysis of the Stretch-Twist-Fold Flow System in a Fractional Order

Sardar Rashid Fattah[1*], Niazy Hady Hussein[2], and Sheelan Abdulkader Osman[1]

[1]Department of Mathematics, Faculty of Science, Soran University, Kawa St.-Soran, Erbil, Iraq
[2]Department of Mathematics, College of Education, Salahadin University-Erbil, Erbil ,Kurdistan, Iraq

ABSTRACT

This study investigates a modified fractional Stretch-Twist-Fold (STF) model with a Caputo fractional-order derivative. The local stability and Hopf bifurcation of equilibrium points are analyzed by using an Adams-type predictor-corrector method implemented in MATLAB software. We study the influence of variation of parameters on the system's behavior and verify chaotic dynamics by computing maximal Lyapunov exponents. In addition to supporting analytical findings, numerical simulations are used to reveal chaotic characteristics such as bifurcations, phase portraits, limit cycles, and attractive chaotic sets, highlighting the crucial role of the fractional-order derivative in the system's dynamic behavior.

1.Introduction

Fractional calculus is a field within applied mathematics that focuses on derivatives and integrals of fractional order. Although fractional derivatives have been around for over three centuries, their development was slow due to a lack of geometric interpretation and practical applications. However, in recent decades, it has attracted significant interest from researchers in various disciplines, such as engineering, economics, secure communications, and so on (Lyubomudrov, Edelman et al., 2003; Kiani-B, Fallahi et al., 2009; Sheu, Chen et al., 2010; Tenreiro Machado, Eugénia Mata et al., 2015; Machado and Galhano, 2018). The efficiency of fractional derivatives primarily stems from their non-local and history-dependent nature, which takes into account the entire history of a process at any given moment rather than just its current state. Thus, fractional calculus will be an effective and proper tool for investigating the memory and hereditary features of materials and processes. The usefulness of fractional derivatives appears in the modeling of the mechanical and electrical characteristics of actual materials (Podlubny, 1998). Furthermore, many new fractional-order systems in various fields have been introduced recently, exhibiting rich and complex dynamics, including periodic solutions, bifurcations, and chaotic phenomena. For instance, Uddin established the existence and direction of Neimark-Sacker and flip bifurcations in the Brusselator model by employing the central manifold (Uddin, 2022). Cuiyan Wang et al. presented rich bifurcation and chaos behavior by investigating a fractional-order Duffing system with time delay (Wang, Wang et al., 2023). Bhalekar and Gupta presented bifurcations in fractional-order delay differential equations of cubic nonlinearity (Bhalekar and Gupta, 2022). Suryanto et al. investigated discrete-time fractional-order predator–prey models using center manifold theory and bifurcation analysis (Suryanto, Darti et al., 2025). Chettouh and Menacer investigated the effects of fractional order on the stability and localization of the critical Hopf bifurcation value in a chaotic jerk system (Chettouh and Menacer, 2024). In addition, Abualhomos et al. exhibited hidden attractors and intricate bifurcations in discrete fractional memristive maps (Abualhomos, Abbes et al., 2023). Danca explored fractional-order map symmetry-breaking bifurcations (Danca, 2023), while Edelman et al. explored the onset of chaos in generalized fractional maps of order $(0 < \omega < 1)$ (Edelman, Helman et al., 2023). Wang et al. conducted an exploration of Hopf bifurcations in fractional-order delayed memristor-based chaotic circuits, conclusively discovering transitions to chaotic dynamics when the fractional order or time delay exceeds specific critical values (Hu, Ding et al., 2017). Kaslik and Sivasundaram studied fractional-order biological systems and showed how fractional derivatives influence the occurrence of Hopf bifurcations and the resulting oscillations (Kaslik and Sivasundaram, 2012). Global numerical methods are used to determine the boundary and interior crises in a system of fractional differential equations (Liu, Hong et al., 2016; Osman and Langlands, 2022). The field received new impetus from papers proposing new chaotic systems (Sprott, 2011) and reporting on simple chaotic flows in a plane of equilibria (Jafari, Sprott et al., 2016). Such results highlight the importance of fractional-order modeling for the development of contemporary bifurcation theory and nonlinear dynamics. Moreover, bifurcation theory studies the qualitative or topological properties of fractional differential systems, including equilibria, periodic solutions, homoclinic and heteroclinic orbits, and invariant tori, when suitable values of parameters in the nonlinear models of complexity dynamics are assumed. Poincaré's pioneering work in 1892 (Poincaré, 1893) foreshadowed this endeavor. Researchers have long studied bifurcations in fractional-order systems, primarily focusing on changing one of the system parameters or a predefined derivative order. Some of the work has focused on bifurcation when, at the same time, a system parameter and the derivative of a particular order are changed (Cafagna and Grassi, 2008; El-Saka, Ahmed et al., 2009; Liu and Hong, 2013; Leung, Yang et al., 2014; Ji, Lai et al., 2018). Hopf bifurcation is a specific type of bifurcation that occurs when two complex eigenvalues of the Jacobian matrix cross the imaginary axis at an

equilibrium point, causing a change in the point's stability. In particular, as a bifurcation parameter passes through a critical value, the equilibrium points change from stable to unstable (Xiao and Zheng, 2012; Deshpande, Daftardar-Gejji et al., 2017). Besides, fractional-order chaotic systems exhibit more complex dynamic behaviors and offer more variables for adjustment compared to their integer-order counterparts. This paper builds on the approach of previous studies by presenting and examining a similar fractional-order version of a generalized stretch-twist-fold flow system (see Section 3). The system's dynamics are investigated for commensurate fractional order $\omega \in (0,1)$. This article not only presents proof of Hopf bifurcations and chaos but also verifies their existence by using numerical simulations based on the Adams-type predictor-corrector method.

The remainder of the paper is organized as follows: Section 2 presents an overview of fractional calculus, including basic concepts and further information on the stability of fractional dynamic systems. The fractional-order modified stretch-twist-fold (STF) system, as investigated by Bao and Yang (Bao and Yang, 2014), is presented in Section 3. The Hopf bifurcation at each equilibrium point is examined in Section 4. The chaotic dynamics of the proposed fractional-order STF system are analyzed in Section 5. The main conclusions of the research are summarized in Section 6.

2 Preliminaries

In this section, we introduce the essential concepts, definitions, and stability conditions of fractional-order systems that are required throughout the paper. Several standard definitions are used in fractional calculus in the literature; see (Podlubny, 1998; Diethelm and Ford, 2010). We summarize those most relevant to our study.

2.1 Fundamental Definitions in Fractional Calculus

Definition 2.1.1. (Podlubny, 1998; Kilbas, Srivastava et al., 2006; Das, 2011) Fractional calculus extends the concepts of integration and differentiation. The mathematical equation that defines the operator in fractional calculus has been established by

$$ {}_{t_0}D_t^{\omega} = \begin{cases} \dfrac{d^{\omega}}{dt^{\omega}}, & \text{if } \omega > 0, \\ 1, & \text{if } \omega = 0, \\ \displaystyle\int_{t_0}^{t} (d\tau)^{\omega}, & \text{if } \omega < 0, \end{cases} \quad (1) $$

where $\omega \in \mathbb{R}$ denotes the fractional order, and t_0 and t stand for the integral's bottom and upper limits, respectively.

Definition 2.1.2. (Podlubny, 1998; Kilbas, Srivastava et al., 2006; Das, 2011) The Caputo fractional order derivative of a function $g(t)$ is defined as follows:

$$ {}_{t_0}^{C}D_t^{\omega} g(t) = $$

$$ \begin{cases} \dfrac{1}{\Gamma(m-\omega)} \displaystyle\int_{t_0}^{t} (t-\psi)^{m-\omega-1} g^{(m)}(\psi) d\psi, & \\ & m-1 < \omega < m, \quad (2) \\ \dfrac{d^m}{dt^m} g(t), & \omega = m, \end{cases} $$

where ${}_{t_0}^{C}D_t^{\omega}$ is the operator for the Caputo derivative of order ω, $m-1 < \omega < m$, $m \in \mathbb{N}$, and the parameter t_0 denotes the initial time. The gamma function $\Gamma(m-\omega)$ is represented by the integral $\Gamma(m-\omega) = \int_0^{\infty} t^{(m-\omega)-1} e^{-t} d$.

Definition 2.1.3. (Podlubny, 1998; Kilbas, Srivastava et al., 2006; Das, 2011) For a function $g(t)$, the fractional integral of order $\omega > 0$ is defined as follows:

$$ {}_{t_0}I_t^{\omega} g(t) = \frac{1}{\Gamma(\omega)} \int_{t_0}^{t} (t-\psi)^{\omega-1} g(\psi) d\psi. \quad (3) $$

The fractional integral operator ${}_{t_0}I_t^{\omega}$ possesses the following three fundamental properties:

$$ {}_{t_0}I_t^{\omega} (t-t_0)^{\sigma} = \frac{\Gamma(\sigma+1)}{\Gamma(\sigma+1+\omega)} (t-t_0)^{\sigma+\omega}, \quad (4) $$

$$ {}_{t_0}I_t^{\omega} W = \frac{W}{\Gamma(\omega+1)} (t-t_0)^{\omega}, \quad (5) $$

$$ {}_{t_0}I_t^{\omega} {}_{t_0}I_t^{v} g(t) = {}_{t_0}I_t^{\omega+v} g(t). \quad (6) $$

In this context, t_0 represents the initial time, $\omega \geq 0$, $v \geq 0$, $\sigma > -1$, and W is a real-valued

constant.

During this investigation, for fractional derivative, we use the Caputo definition with fractional order, where $\omega \in (0,1]$.

2.2 Numerical Methods

The predictor-corrector method was first introduced by Diethelm et al. (Diethelm, Ford et al., 2002) and is used to solve the fractional-order differential system discussed in this paper. This method is suitable for solving fractional differential equations with initial value problems. Furthermore, it helps us to numerically simulate the system dynamics and verify the validity of the theoretical findings, which will be presented in the following sections.

We consider the following fractional differential equation with initial conditions:

$$\frac{d^{\omega}y}{dt^{\omega}} = g(t,y), \quad 0 \le t \le L, \tag{7}$$

$$y^{l}(0) = y_0^{(l)}, \quad l = 0,1,\dots,\lceil\omega\rceil - 1, \quad \omega \in (0,1).$$

The equation (7) corresponds to the Volterra integral equation, see section 2 in (Diethelm, Ford et al., 2002):

$$y(t) = \sum_{l=0}^{\lceil\omega\rceil-1} y_0^{(l)} \frac{t^l}{l!} + \frac{1}{\Gamma(\omega)} \int_0^t (t-\psi)^{(\omega-1)} g(\psi, y(\psi)) d\psi. \tag{8}$$

We discretize the interval [0, L] into m subintervals of size $h = L/m$, and define $t_\epsilon = \epsilon h$, for $\epsilon = 0,1,\dots,m$. Then the corrector formula for equation (8) can be described as follows (see (Diethelm, Ford et al., 2002), pages 3-6 for full details):

$$y_h(t_{m+1}) = \sum_{l=0}^{\lceil\omega\rceil-1} y_0^{(l)} \frac{t_{m+1}^l}{l!} + \frac{h^{\omega}}{\Gamma(\omega+2)} g\left(t_{m+1}, y_h^p(t_{m+1})\right) + \frac{h^{\omega}}{\Gamma(\omega+2)} \sum_{\epsilon=0}^{m} \phi_{\epsilon,m+1} g\left(t_\epsilon, y_h(t_\epsilon)\right), \tag{9}$$

where the predictor values $y_h(t_{m+1})$ are computed using the approach presented in (Diethelm, Ford et al., 2002),

$$y_h^p(t_{m+1}) = \sum_{l=0}^{\lceil\omega\rceil-1} y_0^{(l)} \frac{t_{m+1}^l}{l!} + \frac{1}{\Gamma(\omega)} \sum_{\epsilon=0}^{m} \Omega_{\epsilon,m+1} g\left(t_\epsilon, y_h(t_\epsilon)\right), \tag{10}$$

where the weights $\phi_{\epsilon,m+1}$ and $\Omega_{\epsilon,m+1}$, as defined in (Diethelm, Ford et al., 2002), are given by the following formulas:

$$\phi_{\epsilon,m+1} = \begin{cases} m^{\omega+1} - (m-\omega)(m+1)^{\omega}, & \epsilon = 0 \\ (m-\epsilon+2)^{\omega+1} + (m-\epsilon)^{\omega+1} & \\ -2(m-\epsilon+1)^{\omega+1}, & 1 \le \epsilon \le m \\ 1, & \epsilon = m+1 \end{cases} \tag{11}$$

and

$$\Omega_{\epsilon,m+1} = \frac{h^{\omega}}{\omega}\left((m-\epsilon+1)^{\omega} - (m-\epsilon)^{\omega}\right), 1 \le \epsilon \le m. \tag{12}$$

2.3 Stability of the Fractional Differential systems

In this subsection, we discuss the necessary conditions for a general fractional-order system to be stable. First, we will consider the following fractional-order differential systems:

$$\begin{aligned} {}_{t_0}^{C}D_t^{\omega_i} y_i(t) &= g_i(y_1(t), y_2(t), \dots, y_m(t), t), \\ y_i(0) &= y_i, \quad \text{for } i = 1,\dots,m. \end{aligned} \tag{13}$$

The system structure and associated stability condition are discussed in (Matignon, 1996; Ahmed, El-Sayed et al., 2007; Tavazoei and Haeri, 2009). The Jacobian matrix structure of the fractional-order system (13) assessed at the equilibrium point $E^* = (y_1^*, y_2^*, \dots, y_m^*)$ is determined as

$$J = \left[\frac{\partial g_i}{\partial y_j}\right], \quad \text{for } i = 1,\dots,m \text{ and } j = 1,\dots,m. \tag{14}$$

Definition 2.3.1. (Tavazoei and Haeri, 2008) Consider the fractional-order system (13), where the current state vector is written as $\mathbf{y} = (y_1, y_2, \dots, y_m)^T$, and the vector that shows the orders of the fractional derivatives is $\omega = (\omega_1, \omega_2, \dots, \omega_m)^T$, with each $\omega_j > 0$, for $j = 1,\dots,m$.

When all of the derivatives' orders are the same, the system is known as a commensurate-order system, meaning ($\omega_1 = \omega_2 = \cdots = \omega_m$); if they are not the same, it is referred to as an incommensurate-order system.

Definition 2.3.2. (Bandyopadhyay and Kamal, 2015) A point E^* is defined as an equilibrium point of system (13) exactly when it satisfies the condition $g_j(t, E^*) = 0$; for $j = 1, \ldots, m$.

Theorem 2.3.1. (Ghaziani, Alidousti et al., 2016) Let $J(E^*)$ represent the Jacobian matrix of fractional-order system (13) assessed at the equilibrium point E^*. The eigenvalues of $J(E^*)$ are denoted by λ_j, where $j = 1, \ldots, m$. The equilibrium point E^* is classified as a saddle point when certain eigenvalues fulfill $|\arg(\lambda_j)| > \frac{\omega\pi}{2}$, whereas others meet $|\arg(\lambda_j)| < \frac{\omega\pi}{2}$.

Theorem 2.3.2. (Ghaziani, Alidousti et al., 2016) Considering the commensurate fractional-order system (13), the equilibrium point E^* is locally asymptotically stable if each eigenvalue λ_j of the Jacobian matrix $J(E^*)$ possesses angles exceeding $\frac{\omega\pi}{2}$, precisely $|\arg(\lambda_j)| > \frac{\omega\pi}{2}$. If the previous requirement is not met, the equilibrium point E^* is unstable.

From the above Theorem, the stability region of the fractional-order system (13), for $0 < \omega < 1$, is shown in Figure 1.

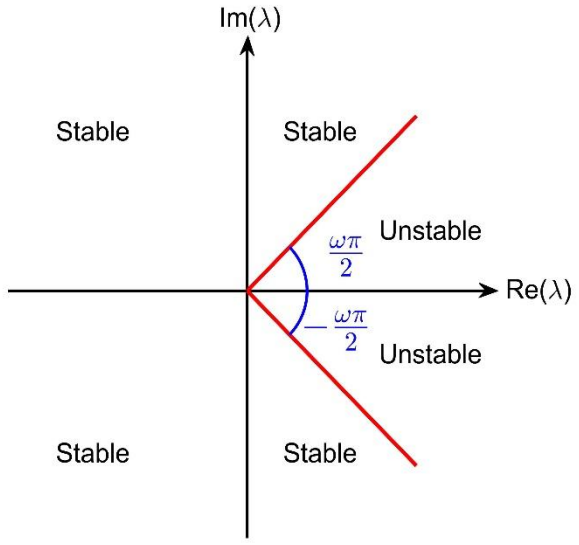

Figure 1: Region of stability in the fractional-order system (13).

3 The Fractional Stretch-Twist-Fold System

In this section, we present a fractional-order version of a Stretch-Twist-Fold (STF) flow system, which represents the original contribution of this research. The aim in this study is to extend the integer-order STF model by applying the Caputo fractional derivative with commensurate order, thereby demonstrating the system's complex behaviors more effectively, such as Hopf bifurcation and chaotic dynamics. Additionally, our work in this section begins by finding the equilibrium points of the system, computing the Jacobian matrix, and deriving the characteristic equation. These analyses form the foundation for understanding the local stability and behavior of the fractional-order STF system we propose, which we will utilize later in the paper to demonstrate that a Hopf bifurcation occurs in Section 4 and that the system exhibits chaotic behavior in Section 5.

The stretch–twist–fold (STF) flow exemplifies an indestructible steady Stokes flow that simulates the processes of stretching, twisting, and folding. Vainshtein and Zel'dovich first presented the STF flow in 1972 during their examination of a rapid dynamo within magnetohydrodynamics (Vainshtein and Zel'dovich, 1972), and this flow proficiently delineates the intrinsic enhancement of magnetic field intensity produced by electrically conductive fluids in astrophysical scenarios (Moffatt, 1989; Childress and Gilbert, 2008). The studies on the physical and dynamic features of STF flow have persisted for many decades due to its extensive application across several domains (Vainshtein, Sagdeev et al., 1996; Vainshtein, Sagdeev et al., 1997; Asgari-Targhi and Berger, 2009; Bao and Yang, 2010; Yue and Aqeel, 2013; Bao and Yang, 2014; Maciejewski and Przybylska, 2020). Numerous research studies have presented enhanced models using supplementary parameters to examine bifurcations and chaotic phenomena related to STF flow (Bao and Yang, 2014; Azam, Aqeel et al., 2017; Hussein and Amen, 2019). Before introducing the modified system, we note that under standard conditions, specifically when the right-hand side of the system is continuous and satisfies a Lipschitz condition, the existence and uniqueness of solutions to the fractional-

order system are guaranteed, see (Podlubny, 1998). These conditions are fulfilled in our scenario, ensuring that the fractional-order initial value problem is well-posed. The integer-order STF system is given by the following three equations:

$$\begin{aligned} \dot{x} &= r_1 z - 8(d+1)xy\,, \\ \dot{y} &= 11x^2 + 3y^2 + z^2 + r_2 xz - 3c^2, \\ \dot{z} &= -r_1 x + 2yz - r_2 xy, \end{aligned} \tag{15}$$

where (r_1, r_2, d, c) ∈ R , r_1>0 and r_2>0.

For $d = 0$ and $c = \pm 1$, system (15) reduces to the original STF flow (Bajer, 1989).

Applying Definition 2.1.2, the commensurate fractional-order modified STF flow (15) is

$$\begin{aligned} {}_{t_0}^{C}D_t^{\omega} x &= r_1 z - 8(d+1)xy, \\ {}_{t_0}^{C}D_t^{\omega} y &= 11x^2 + 3y^2 + z^2 + r_2 xz - 3c^2, \\ {}_{t_0}^{C}D_t^{\omega} z &= -r_1 x + 2yz - r_2 xy, \end{aligned} \tag{16}$$

where $0 < \omega \leq 1$ with the initial conditions $(x(0), y(0), z(0)) = (x_0, y_0, z_0)$.

Unlike (Bao and Yang, 2014), we identify all equilibrium points. By using Definition 2.3.2, ${}_{t_0}^{C}D_t^{\omega} x = {}_{t_0}^{C}D_t^{\omega} y = {}_{t_0}^{C}D_t^{\omega} z$ =0, the equilibrium points of the fractional-order STF system (16) can be determined via the solution of the following calculation:

$$r_1 z - 8(d+1)xy = 0, \tag{17}$$
$$11x^2 + 3y^2 + z^2 + r_2 xz - 3c^2 = 0, \tag{18}$$
$$-r_1 x + 2yz - r_2 xy = 0, \tag{19}$$

From equation (17), we express z in terms of x and y; this implies

$$z = \frac{8(d+1)xy}{r_1}. \tag{20}$$

By substituting z into equation (18) and simplifying, then

$$11x^2 + 3y^2 + \frac{64(d+1)^2 x^2 y^2}{r_1^2} + \frac{8r_2(d+1)x^2 y}{r_1} - 3c^2 = 0. \tag{21}$$

Solving the above equation to find the value of x

$$x = \pm \sqrt{\frac{r_1^2(3c^2 - 3y^2)}{11r_1^2 + 64(d+1)^2 y^2 + 8r_1 r_2 (d+1)y}}, \tag{22}$$

again, substituting z from equation (20) into equation (19), after simplifying, we get

$$-r_1 x + \frac{16(d+1)xy^2}{r_1} - r_2 xy = 0, \tag{23}$$

this implies either:

$$x = 0 \text{ or } -r_1 + \frac{16(d+1)y^2}{r_1} - r_2 y = 0. \tag{24}$$

If $x = 0$, then substituting into equation (21) to obtain values of y, it becomes $y = \pm c$.
To find the value of z in this case, we substitute $y = \pm c$ into equation (20), which allows us to determine the result as follows:

$$z = \frac{8(d+1)(0)(\pm c)}{r_1} = 0. \tag{25}$$

Therefore, we have two equilibrium points in the first case: $E_{1,2} = (0, \pm c, 0)$.
If $-r_1 + \frac{16(d+1)y^2}{r_1} - r_2 y = 0$, then multiply both sides by r_1

$$16(d+1)y^2 - r_1 r_2 y - r_1^2 = 0, \tag{26}$$

the above equation is structured as a quadratic equation in terms of y; solving it yields

$$y = \frac{r_1\left(r_2 \pm \sqrt{r_2^2 + 64(d+1)}\right)}{32(d+1)}. \tag{27}$$

it follows that d can be expressed as $d = \frac{k^2 - r_2^2}{64} - 1$.
By substituting this assumption into equation (27), the value of y will become

$$y = \frac{2r_1(r_2 \pm k)}{(k^2 - r_2^2)}. \tag{28}$$

To find x, we substitute y from equation (28) into equation (22), and after simplifying, we conclude

$$x = \pm\sqrt{\frac{(3c^2(r_2^2-k^2)^2 - 12r_1^2(r_2 \pm k)^2)16}{(r_2^2-k^2)^2\big(176+(r_2 \pm k)^2+4r_2(r_2 \pm k)\big)}}. \tag{29}$$

Substituting the value of x from equation (29) and y from equation (28) into equation (20) to find the value of z

$$z = (r_2 \pm k)\left(\pm\sqrt{\frac{(3c^2(r_2^2-k^2)^2 - 12r_1^2(r_2 \pm k)^2)}{(k^2-r_2^2)^2\big(176+(r_2 \pm k)^2+4r_2(r_2 \pm k)\big)}}\right). \tag{30}$$

Therefore, the equilibrium points of the second case are

$$\left(\pm\sqrt{\frac{(3c^2(r_2^2-k^2)^2 - 12r_1^2(r_2 \pm k)^2)16}{(r_2^2-k^2)^2\big(176+(r_2 \pm k)^2+4r_2(r_2 \pm k)\big)}}, -\frac{2r_1(r_2 \pm k)}{(r_2^2-k^2)}\right.$$
$$\left.(r_2 \pm k)\left(\pm\sqrt{\frac{(3c^2(r_2^2-k^2)^2 - 12r_1^2(r_2 \pm k)^2)}{(r_2^2-k^2)^2\big(176+(r_2 \pm k)^2+4r_2(r_2 \pm k)\big)}}\right)\right).$$

By separating and simplifying all the equilibrium points in this case, we get

$$E_3 = \left(\frac{4\sqrt{3}}{(r_2-k)}\sqrt{\frac{(r_2-k)^2c^2-4r_1^2}{5r_2^2+6r_2k+k^2+176}}, \frac{-2r_1}{(r_2-k)}, \frac{\sqrt{3}(r_2+k)}{(r_2-k)}\left(\sqrt{\frac{(r_2-k)^2c^2-4r_1^2}{5r_2^2+6r_2k+k^2+176}}\right)\right).$$

$$E_4 = \left(\frac{-4\sqrt{3}}{(r_2-k)}\sqrt{\frac{(r_2-k)^2c^2-4r_1^2}{5r_2^2+6r_2k+k^2+176}}, \frac{-2r_1}{(r_2-k)}, \frac{-\sqrt{3}(r_2+k)}{(r_2-k)}\left(\sqrt{\frac{(r_2-k)^2c^2-4r_1^2}{5r_2^2+6r_2k+k^2+176}}\right)\right).$$

$$E_5 = \left(\frac{4\sqrt{3}}{(r_2+k)}\sqrt{\frac{(r_2+k)^2c^2-4r_1^2}{5r_2^2-6r_2k+k^2+176}}, \frac{-2r_1}{r_2+k}, \frac{\sqrt{3}(r_2-k)}{(r_2+k)}\left(\sqrt{\frac{(r_2+k)^2c^2-4r_1^2}{5r_2^2-6r_2k+k^2+176}}\right)\right).$$

$$E_6 = \left(\frac{-4\sqrt{3}}{(r_2+k)}\sqrt{\frac{(r_2+k)^2c^2-4r_1^2}{5r_2^2-6r_2k+k^2+176}}, \frac{-2r_1}{(r_2+k)}, \frac{-\sqrt{3}(r_2-k)}{(r_2+k)}\left(\sqrt{\frac{(r_2+k)^2c^2-4r_1^2}{5r_2^2-6r_2k+k^2+176}}\right)\right).$$

Therefore, the set of the equilibrium points of the system (16) are

$$E_{1,2} = (0, \pm c, 0).$$

$$E_{3,4} = \left(\pm\frac{4\sqrt{3}}{A}\sqrt{\frac{C}{H}}, -\frac{2a_1}{A}, \pm\frac{\sqrt{3}B}{A}\sqrt{\frac{C}{H}}\right).$$

$$E_{5,6} = \left(\pm\frac{4\sqrt{3}}{B}\sqrt{\frac{D}{F}}, -\frac{2a_1}{B}, \pm\frac{\sqrt{3}A}{B}\sqrt{\frac{D}{F}}\right).$$

$$Where,\ A = r_2 - k,\ B = r_2 + k,$$

$$C = (r_2-k)^2c^2 - 4r_1^2,$$
$$D = (r_2+k)^2c^2 - 4r_1^2,$$

$H = 5r_2^2 + 6r_2k + k^2 + 176,\ F = 5r_2^2 - 6r_2k + k^2 + 176,\ k = \pm\sqrt{r_2^2 + 64(d+1)}.$

The equilibrium points are all real and exist, where $\frac{C}{H} \geq 0,\ \frac{D}{F} \geq 0,\ A \neq 0,\ and\ B \neq 0$. Furthermore, the results of the equilibrium points are original and based on our calculations, without reference to any prior work.

Under the transformation $d = \frac{k^2 - r_2^2}{64} - 1$, the fractional-order system (16) becomes

$$\begin{aligned} {}_{t_0}^{C}D_t^{\omega}x &= r_1 z - \frac{1}{8}(k^2 - r_2^2)xy, \\ {}_{t_0}^{C}D_t^{\omega}y &= 11x^2 + 3y^2 + z^2 + r_2xz - 3c^2\,, \\ {}_{t_0}^{C}D_t^{\omega}z &= -r_1x + 2yz - r_2xy. \end{aligned} \quad (31)$$

This system will be used in the following sections to study the local stability, Hopf bifurcation, and chaotic behavior. The Jacobian matrix based at the equilibrium point $E = (x, y, z)$ is

$$J_E = \begin{bmatrix} -\frac{(k^2 - r_2^2)y}{8} & -\frac{(k^2 - r_2^2)x}{8} & r_1 \\ r_2z + 22x & 6y & r_2x + 2z \\ -r_2y - r_1 & -r_2x + 2z & 2y \end{bmatrix}, (32)$$

and the corresponding characteristic polynomial is of the following form:

$$P_E(\lambda) = \lambda^3 + \eta\lambda^2 + \varphi\lambda + \Delta,$$

where λ denotes the eigenvalue of the system, and

$$\eta = -8y - \frac{1}{8}r_2^2y + \frac{1}{8}k^2y,$$

$$\varphi = -\tfrac{1}{8}r_2^3xz + r_1r_2y + 12y^2 - 4z^2 + r_1^2 + \tfrac{1}{8}r_2k^2xz - \tfrac{7}{4}r_2^2x^2 + r_2^2y^2 - k^2y^2 + \tfrac{11}{4}k^2x^2,$$

$$\begin{aligned} \Delta =& \tfrac{1}{2}r_2^3xyz + \tfrac{5}{4}r_1r_2^2xz - \tfrac{1}{8}r_1r_2k^2x^2 - \tfrac{1}{4}r_1k^2xz - \tfrac{3}{2}r_2^2y^3 + \tfrac{3}{2}k^2y^3 - 6r_1^2y - \tfrac{1}{2}r_2k^2xyz + \tfrac{1}{2}r_2^2yz^2 \\ & - \tfrac{1}{2}k^2yz^2 + \tfrac{11}{2}r_2^2x^2y - \tfrac{11}{2}k^2x^2y + 22r_1r_2x^2 - 2r_1r_2z^2 - 44r_1xz + \tfrac{1}{8}r_1r_2^3x^2 - 6r_1r_2y^2. \end{aligned}$$

Selecting suitable values for the parameters in the system employed can help to determine the stability region and demonstrate the occurrence of Hopf bifurcation. Under certain fractional order conditions, the analysis verifies that the system transitions from stable to unstable dynamics. Thus, the system displays chaotic behavior. These findings demonstrate the fundamental importance of a fractional order in the system's dynamics. Further details will be provided in the subsequent sections.

4 Hopf Bifurcations for the Fractional STF System

In this section, we focus on the long-term behavior of trajectories, disregarding transient states. Although the limit cycle resulting from a Hopf bifurcation does not represent an exact solution of the fractional-order system, it serves as an attractor for nearby solutions. Several studies have investigated the presence of Hopf bifurcations in fractional-order systems (Abdelouahab, Hamri et al., 2012; Li and Wu, 2014). Also, this study adopts the criterion for the occurrence of a Hopf bifurcation proposed by Xiang Li and Ranchao Wu (Li and Wu, 2014). Furthermore, the stability of the fractional-order system is strongly influenced by the fractional order ω , which is regarded as a bifurcation parameter in the system. We define the function g with respect to ω as follows:

$$g(\omega) = \frac{\omega\pi}{2} - \min_{1 \leq j \leq 3} \left|\arg(\lambda_j)\right|.$$

Where ω denotes the fractional order as the bifurcation parameter of the given system, and λ_j's are the eigenvalues of the Jacobian matrix of the fractional-order system (31). Additionally, an equilibrium point is locally asymptotically stable if $g(\omega) < 0$ and unstable if $g(\omega) > 0$. The subsequent theorem is necessary to examine the Hopf bifurcation of fractional-order differential systems.

Theorem 4.1. (Li and Wu, 2014) (Conditions for the occurrence of Hopf bifurcation) The fractional-order STF system shows a Hopf bifurcation at the equilibrium point when the

bifurcation parameter ω passes through the critical value $\omega^* \in (0,1)$, provided that the following criteria are satisfied:

i. The Jacobian matrix of system (31) at the equilibrium point has two complex conjugate eigenvalues $\lambda_{1,2} = \rho \pm i\mu$, where $\rho > 0$, $\mu \neq 0$, and one negative real eigenvalue λ_3.

ii. $g(\omega^*) = 0$, $\left(\omega^* = \frac{2}{\pi}\left|\arg\left(\lambda_{1,2}\right)\right|\right)$,

iii. $\frac{d[g(\omega)]}{d\omega}\Big|_{\omega=\omega^*} \neq$, (Condition of transversality).

So, the equilibrium point is locally asymptotically stable for $\omega \in (0, \omega^*)$ and is unstable when $\omega \in (\omega^*, 1)$. Also, Hopf bifurcation occurs at $\omega = \omega^*$.

To ensure that Hopf bifurcation occurs at the equilibrium points $E_{1,2}$, similar to (Bao and Yang, 2014), we will determine the range of parameters based on the first condition of Theorem 4.1, which states that the eigenvalue of the characteristic equation must meet specific criteria. However, these sets of parameter ranges differ from the ones found by Bao and Yang in their paper due to the different structure of eigenvalues. Hopf bifurcation occurs at the equilibrium point $E_1 = (0, -c, 0)$ when parameters are selected from one of the following sets:

$$S_1 = \left\{ r_1 > 0,\ r_2 > 0, 0 < c < \frac{1}{8}\sqrt{r_1^2 r_2^2 + 16 r_1^2} - \frac{r_1 r_2}{8},\quad \sqrt{r_2^2 + 16} < k < \sqrt{16\sqrt{-\frac{r_1 r_2 c - r_1^2}{c^2}} + r_2^2 - 16} \right\}$$

$$S_2 = \left\{ r_1 > 0,\ r_2 > 0, 0 < c < \frac{1}{8}\sqrt{r_1^2 r_2^2 + 16 r_1^2} - \frac{r_1 r_2}{8}, -\sqrt{16\sqrt{-\frac{r_1 r_2 c - r_1^2}{c^2}} + r_2^2 - 16} < k < -\sqrt{r_2^2 + 16} \right\}$$

Furthermore, Hopf bifurcation arises at equilibrium point $E_2 = (0, c, 0)$, when the parameters satisfy the following conditions:

$$S_3 = \left\{ r_1 > 0,\ r_2 > 0, \frac{r_1 r_2}{8} - \frac{1}{8}\sqrt{r_1^2 r_2^2 + 16 r_1^2} < c < 0,\quad \sqrt{r_2^2 + 16} < k < \sqrt{16\sqrt{\frac{r_1^2 + r_1 r_2 c}{c^2}} + r_2^2 - 16} \right\}$$

$$S_4 = \left\{ r_1 > 0,\ r_2 > 0, \frac{r_1 r_2}{8} - \frac{1}{8}\sqrt{r_1^2 r_2^2 + 16 r_1^2} < c < 0, -\sqrt{16\sqrt{\frac{r_1^2 + r_1 r_2 c}{c^2}} + r_2^2 - 16} < k < -\sqrt{r_2^2 + 16} \right\}$$

These ranges of the parameters ensure that the system possesses two complex conjugate eigenvalues, which have a positive real part, and one other negative real eigenvalue, and also appropriate transversality conditions, which allow Hopf bifurcation to emerge at $E_{1,2}$. In the following subsection, we'll determine the fractional order ω using Theorem 2.3.2 and utilize numerical simulations, as presented in Section 2.2, to demonstrate that our system exhibits rich, complex dynamics. We will also determine the range of stability and analyze the Hopf bifurcation for the chosen parameters at all equilibrium points, including the related fractional order at which it occurs; in contrast, Bao and Yang only analyzed the Hopf bifurcation at $E_{1,2}$.

4.1 Numerical Simulation of Hopf Bifurcation in Fractional STF System

This subsection performs a numerical stability analysis to demonstrate that our system undergoes a Hopf bifurcation and to determine the existence of equilibrium points. The goals of these numerical simulations are to illustrate the effects of different parameter values and

variations in the derivative order ω on the dynamic behavior of the fractional-order STF system (31). Without loss of generality, the parameters $r_1 = 20$, $r_2 = 0.1$, $k = 7.59$, and $c = 1$ are considered in the set S_1. The equilibrium points for these parameters are $E_{1,2} = (0, \pm 1, 0)$. First, we consider $E_1 = (0, -1, 0)$, then the Jacobian matrix (32) assessed at this equilibrium point is

$$J_{E_1} = \begin{bmatrix} 7.1998 & 0 & 20 \\ 0 & -6 & 0 \\ -19.9 & 0 & -2 \end{bmatrix}.$$

The characteristic polynomial of J_{E_1} is

$$P_{E_1}(\lambda) = \lambda^3 + 0.8002\lambda^2 + 352.4019\lambda + 2301.602,$$

the eigenvalues are $\lambda_{1,2} = 2.5999 \pm 19.4124i$, $\lambda_3 = -6$,

by applying Theorem 2.3.2, the first equilibrium point E_1 is locally asymptotically stable

where $\left|\arg(\lambda_{1,2})\right| = \tan^{-1}\left(\frac{19.4124}{2.5999}\right) = 1.4377 > \frac{\omega\pi}{2}$,

$0 < \omega < \omega^* < 1$, and unstable when $0 < \omega^* < \omega < 1$.

We can confirm that a Hopf bifurcation occurs at the equilibrium point E_1 when the bifurcation parameter ω passes through the critical value ω^*, i.e., $\omega = \omega^* = 0.915$ (see Figure 2). If ω is greater than ω^*, then the equilibrium point E_1 is unstable. For instance, when we set $\omega = 0.94$, which is greater than ω^*, the equilibrium point E_1 loses its stability (see Figure 3). However, the equilibrium point E_1 is locally asymptotically stable if ω is less than ω^*. In this example, we set $\omega = 0.9$, which is less than $\omega^* = 0.915$; therefore, the equilibrium point E_1 is locally asymptotically stable (see Figure 4). More details are presented in the next section.

From condition (ii) in Theorem 4.1, the critical value parameter ω^* of bifurcation is

$$\omega^* = \frac{2}{\pi}\tan^{-1}\left(\frac{19.4124}{2.5999}\right) \approx 0.915, \text{ and}$$

$$\left.\frac{d[g(\omega)]}{d\omega}\right|_{\omega=\omega^*} = \frac{\pi}{2} \neq 0.$$

Thus, Hopf bifurcation at the equilibrium point E_1 occurs when the bifurcation parameter ω equals its critical value of 0.915.

Second, the equilibrium point $E_2 = (0,1,0)$ is considered; the Jacobian matrix (32) at E_2 of system (31) is

$$J_{E_2} = \begin{bmatrix} -7.1998 & 0 & 20 \\ 0 & 6 & 0 \\ -20.1 & 0 & 2 \end{bmatrix}.$$

The characteristic polynomial of J_{E_2} is

$$P_{E_2}(\lambda) = \lambda^3 - 0.8002\lambda^2 + 356.4019\lambda - 2325.603,$$

and, the eigenvalues are given as $\lambda_{1,2} = -2.5999 \pm 19.5152i$, $\lambda_3 = 6$. According to Theorem 4.1 (Conditions for the occurrence of Hopf bifurcation), a Hopf bifurcation does not occur at the equilibrium point $E_2 = (0, 1, 0)$, because the complex eigenvalues have a negative real part. In contrast, the real eigenvalue is positive. Therefore, the first condition of the theorem is not satisfied.

Furthermore, the parameter values $r_1 = 1.5$, $r_2 = 4$, $k = -2$, and c = 1 are considered for the equilibrium points $E_{3,4}$. The equilibrium points under these parameters are $(\pm 0.4121, -0.5000, \pm 0.2060)$. The Jacobian matrix of the system computed at these equilibrium points is

$$J_{E_{3,4}} = \begin{bmatrix} -0.75 & \pm 0.6181 & 1.5 \\ \pm 9.8900 & -3 & \pm 2.0604 \\ 0.5 & \pm 1.2362 & -1 \end{bmatrix}.$$

Both equilibrium points $E_{3,4}$ share the same characteristic polynomial, which is given by

$$PE_{3,4}(\lambda) = \lambda^3 + 4.75\lambda^2 + 1.6840\lambda + 13.5,$$

then, the eigenvalues are given as $\lambda_{1,2} = 0.1047 \pm 1.6466i$, $\lambda_3 = -4.9593$.

From Theorem 2.3.2, the equilibrium points $E_{3,4}$ are locally asymptotically stable

where $\left|\arg(\lambda_{1,2})\right| = \tan^{-1}\left(\frac{1.6466}{0.1047}\right) = 1.5073 > \frac{\omega\pi}{2}$,

$0 < \omega < \omega^* < 1$, and unstable when $0 < \omega^* < \omega < 1$.

According to the second condition of Theorem 4.1, the critical value parameter ω^* for bifurcation is

$$\omega^* = \frac{2}{\pi}\tan^{-1}\left(\frac{1.6466}{0.1047}\right) \approx 0.96, \text{ and}$$

$$\left.\frac{d[g(\omega)]}{d\omega}\right|_{\omega=\omega^*} = \frac{\pi}{2} \neq 0.$$

We can demonstrate assurance that a Hopf bifurcation occurs at the equilibrium points $E_{3,4}$ when the bifurcation parameter ω reaches the critical point ω^*, i.e., $\omega = \omega^* = 0.96$ (see Figure 5). If $\omega = 0.99 > \omega^*$, then $E_{3,4}$ are unstable (refer to Figure 6). However, the equilibrium points $E_{3,4}$ are locally asymptotically stable when $\omega = 0.9 < \omega^*$ (see Figure 7).

Additionally, if appropriate parameter values are identified at equilibrium points $E_{3,4}$ for a Hopf bifurcation to occur, then by simply changing the sign of the parameter k in the system (31), the resulting equilibrium points $E_{5,6}$ become identical to $E_{3,4}$, without introducing any structural differences. The analysis is demonstrated below: Given the parameters: $r_1 = 1.5$, $r_2 = 4$, $k = 2$, and $c = 1$, the equilibrium points $E_{5,6} = (\pm 0.4121, -0.5000, \pm 0.2060)$, and the Jacobian matrix for the system at $E_{5,6}$ is

$$J_{E_{3,4}} = \begin{bmatrix} -0.75 & \pm 0.6181 & 1.5 \\ \pm 9.8900 & -3 & \pm 2.0604 \\ 0.5 & \pm 1.2362 & -1 \end{bmatrix}.$$

Thus, the eigenvalues of $E_{3,4}$ are the same as those of $E_{5,6}$; therefore, the equilibriums $E_{3,4}$ and $E_{5,6}$ coincide.

4.2 Discussion

The numerical computations were carried out in an attempt to investigate the dynamical behavior of the fractional-order system with various fractional orders $\omega \in (0.9, 1]$. As indicated in Figure 2, the phase space diagram and the corresponding time series exhibit a limit cycle that occurs due to a Hopf bifurcation at the equilibrium point E_1, which is analyzed utilizing the predictor-corrector method. Simulations use initial conditions $(-0.15, -0.92, -0.05)$ and a fractional order of $\omega = 0.915$. The 3D phase space plot demonstrates a limit cycle caused by a Hopf bifurcation around the equilibrium point E_1, as shown in Figure 2(a). Figure 2(b) illustrates a two-dimensional projection onto the xz-plane, highlighting the closed orbital pattern. Also, the trajectories of $x(t), y(t)$, and $z(t)$ over time indicate persistent oscillations due to the Hopf bifurcation at $\omega = 0.915$, as shown in Figure 2(c).

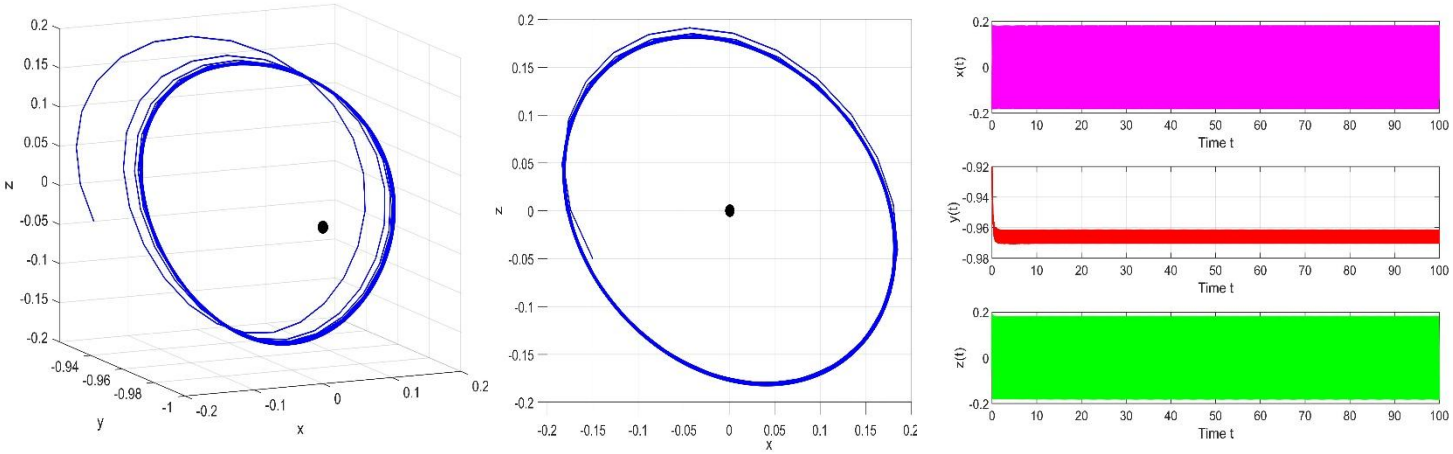

(a) (b) (c)

Figure 2: Phase portrait and time trajectory of fractional-order STF system (31) for $\omega = 0.915$.

Phase space diagram and the time series of the trajectory for fractional order $\omega = 0.94$, with initial conditions $(-0.15, -0.92, -0.05)$ presented in Figure 3, indicate that the system is unstable

at the equilibrium point E_1. Figure 3(a) illustrates the 3D phase space diagram in which an unstable limit cycle diverges from the equilibrium point E_1. Also, a 2D projection onto the xz-plane is shown in Figure 3(b). Furthermore, Figure 3(c) displays the trajectories of $x(t), y(t)$, and $z(t)$ over time, illustrating a departure from the equilibrium point and indicating the onset of unstable dynamics, as well as the trajectory approaching infinity as $t \to \infty$.

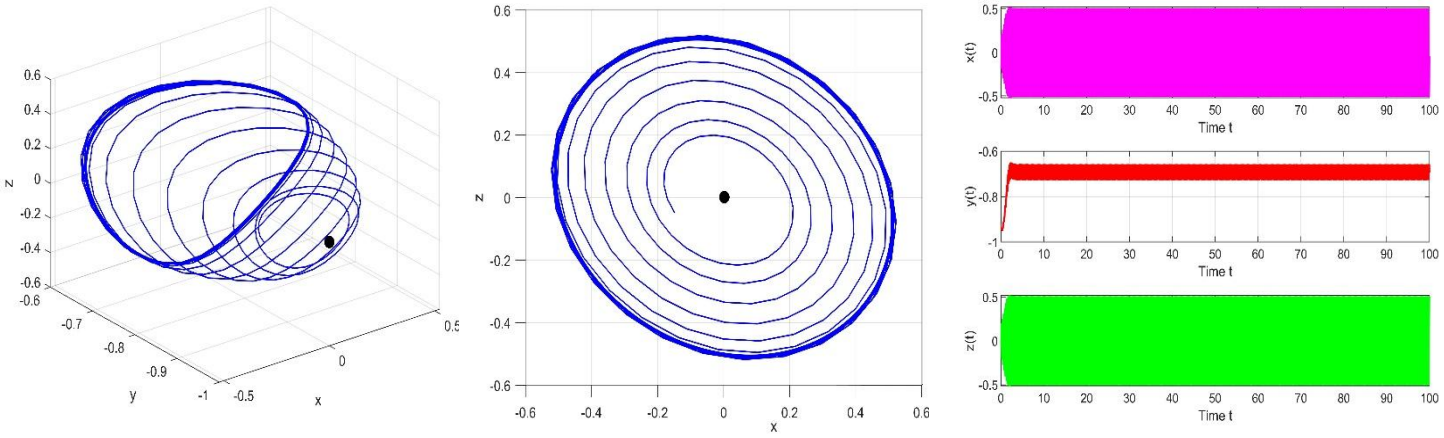

(a) (b) (c)

Figure 3: Phase portrait and time trajectory of fractional-order STF system (31) for $\omega = 0.94$.

In Figure 4, the phase space diagram and the corresponding time series for $\omega = 0.9$ are displayed to indicate local asymptotic stability at the equilibrium point E_1, using the initial conditions $(-0.15, -0.92, -0.05)$. Figure 4(a) shows the 3D phase space diagram where a stable limit cycle converges to the equilibrium point E_1. Additionally, the 2D projection on the xz-plane is demonstrated in Figure 4(b). Also, Figure 4(c) confirms the stable system behavior by demonstrating the trajectories of $x(t), y(t)$, and $z(t)$ for larger values of time and the trajectory approaching E_1 as $t \to \infty$.

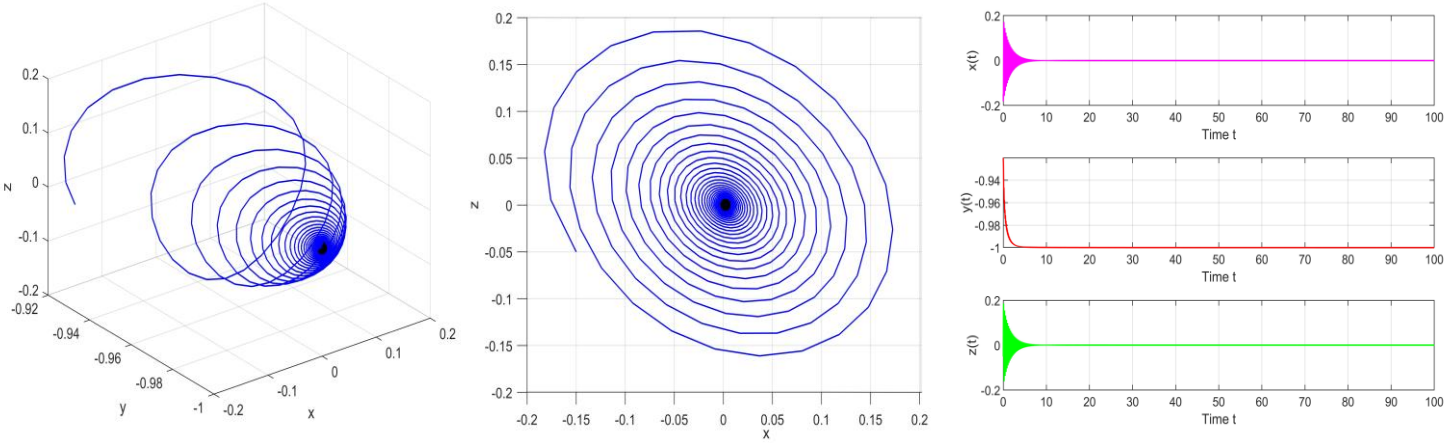

(a) (b) (c)

Figure 4: Phase portrait and time trajectory of fractional-order STF system (31) for $\omega = 0.9$.

In Figure 5, the phase space diagram and the corresponding time series of the fractional-order STF system (31) exhibit a Hopf bifurcation at two symmetric equilibrium points $E_{3,4}$, for $\omega = 0.96$ with initial conditions $(-0.42, -0.49, -0.21)$. The red trajectory corresponds to the solution around the Equilibrium point $E_3 = (0.4121, -0.5000, 0.2060)$, while the blue trajectory illustrates the limit cycle around the symmetric Equilibrium point $E_4 = (-0.4121, -0.5000, -0.2060)$. The 3D phase space diagram displays two visible, symmetrical limit cycles emanating from the equilibrium points $E_{3,4}$, which represent ongoing oscillations resulting from a Hopf bifurcation, as shown in Figure 5(a). Figure 5(b) shows a 2D projection onto the xz-plane. Additionally, in Figure 5(c), the trajectories of $x(t), y(t),$ and $z(t)$ over time illustrate sustained oscillations caused by the Hopf bifurcation at $\omega = 0.9$

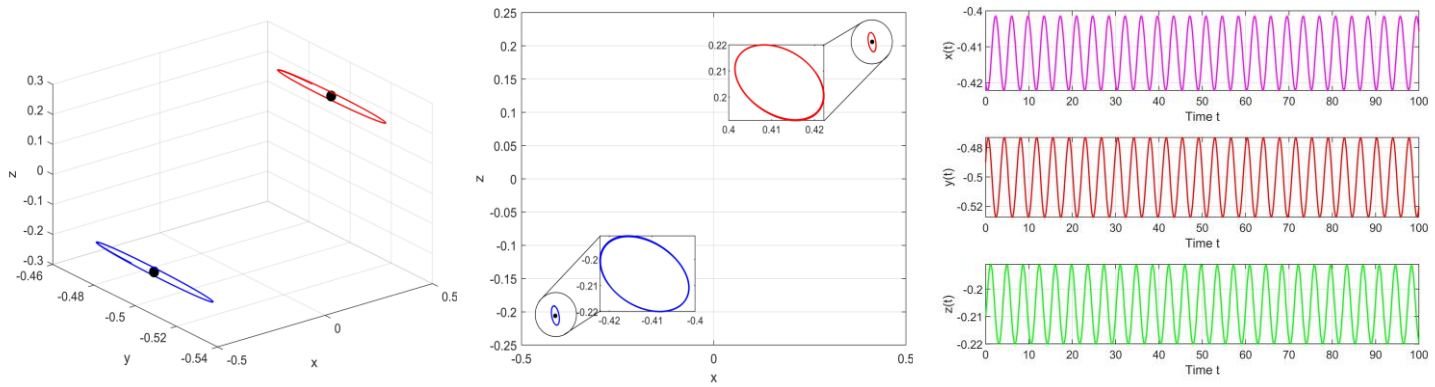

(a) (b) (c)

Figure 5: Phase portrait and time trajectory of fractional-order STF system (31) for $\omega = 0.96$.

In Figure 6, the phase space diagram and the corresponding time series for $\omega = 0.99$ with initial conditions $(-0.42, -0.49, -0.21)$ illustrate instability at equilibrium points $E_{3,4}$. The 3D phase space diagram in Figure 6(a) displays two unstable limit cycles that diverge from the equilibrium points $E_{3,4}$. Figure 6(b) presents the 2D projection onto the xz-plane. Furthermore, the trajectories of $x(t)$, $y(t)$, and $z(t)$ over time indicate a departure from equilibrium points and the onset of unstable dynamics; also, both trajectories approach infinity as $t \to \infty$, demonstrated in Figure 6(c).

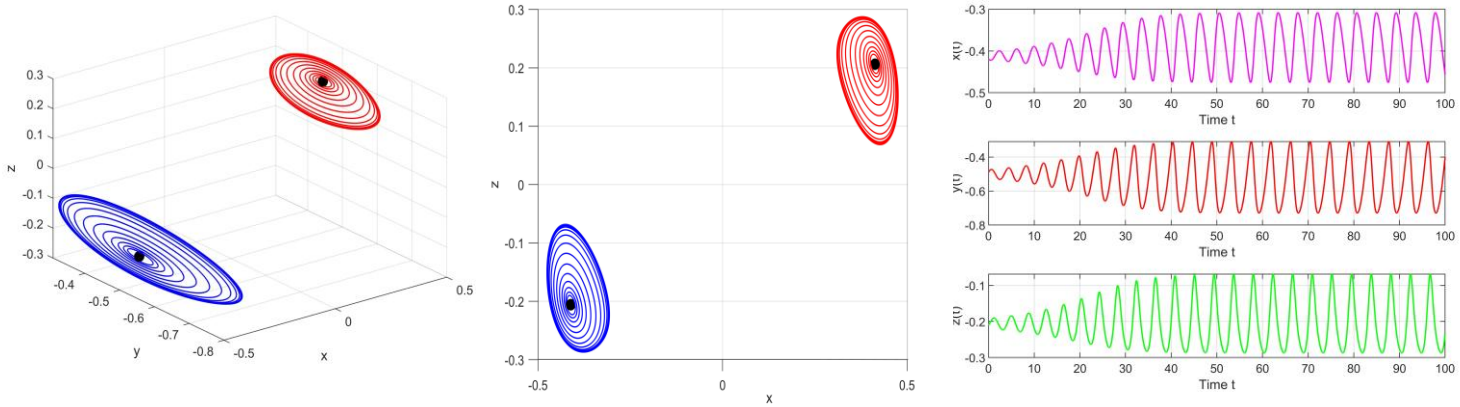

(a) (b) (c)

Figure 6: Phase portrait and time trajectory of fractional-order STF system (31) for $\omega = 0.99$.

In Figure 7, the phase space diagram and the time series for fractional order $\omega = 0.9$ illustrate local asymptotic stability at both symmetric equilibrium points $E_{3,4}$ with initial conditions $(-0.42, -0.49, -0.21)$. The 3D phase space diagram in Figure 7(a) shows two stable limit cycles that converge towards both equilibrium points $E_{3,4}$, indicating that they are locally stable over time. Figure 7(b) shows a 2D projection onto the xz -plane. Furthermore, the trajectories of $x(t), y(t)$, and $z(t)$ over time confirm stable system behavior, as shown in Figure 7(c).

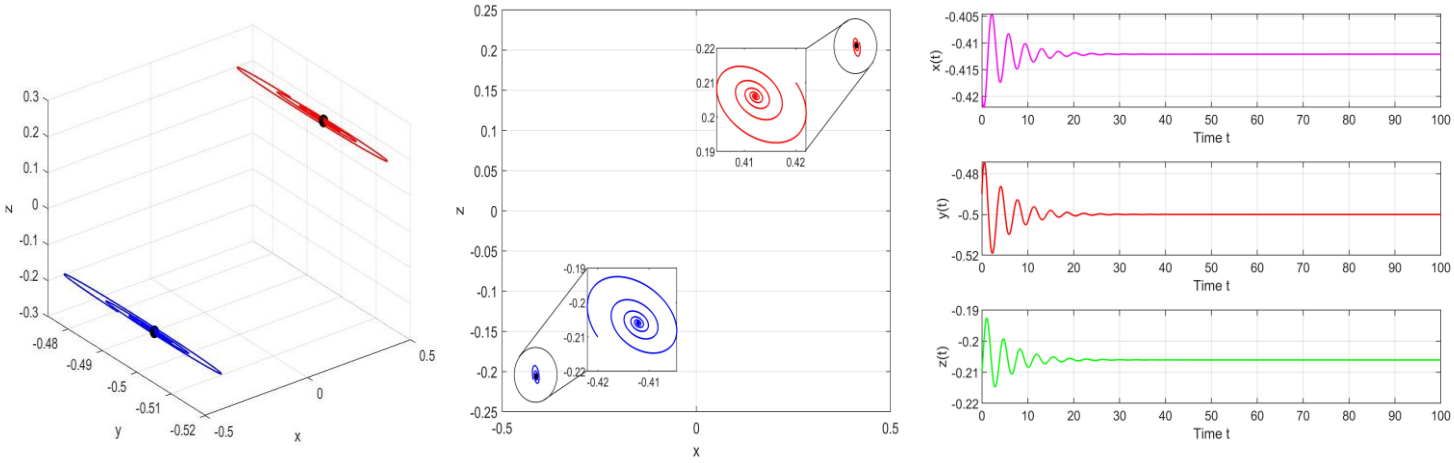

(a) (b) (c)

Figure 7: Phase portrait and time trajectory of fractional-order STF system (31) for $\omega = 0.9$.

4.3 Limitations and Future Improvement in Hopf Bifurcation Analysis

Although the Hopf bifurcation analysis presented in this paper offers important insights into the system's dynamics, some limitations remain, which should be discussed. The bifurcation results primarily depend on numerical simulations that are complemented by linearization techniques, which may not capture all global bifurcation effects across all parameter regimes. Moreover, the predictor-corrector scheme employed for approximating solutions, while efficient, involves discretization errors, which influence accuracy close to critical points of bifurcation. In more studies, the analysis of fractional-order systems can be extended using more robust analytic methods, for example, the center manifold theorem and normal form theory (Zhi, Wajid et al., 2022). These methods can lend a more robust underlying theoretical foundation to the numerical bifurcation outcomes. Further numerical and higher-order techniques can be investigated and used to enhance accuracy and stability in bifurcation detection, particularly at threshold transitions.

5 Chaotic in the Fractional-Order STF System

In this section, we investigate the chaotic behavior of the fractional-order STF system (31) by assigning appropriate parameter values and defining an appropriate fractional order ω. To support the existence of chaos, we utilize two theorems from the literature that identify the required conditions for its occurrence in a fractional-order system. We also confirm these conditions by means of phase portraits and Lyapunov exponents.

Theorem 5.1. (Tavazoei and Haeri, 2007; Tavazoei and Haeri, 2008) To demonstrate chaotic behavior in the fractional-order STF system (31), at least one

eigenvalue $\lambda = \rho \pm i\mu$, must stay in the unstable region. In other words, the presence of instability in the system is a key requirement for the persistence of chaos. Mathematically, the chaotification condition is given by

$$\omega \geq \frac{2}{\pi}\left(\tan^{-1}\left|\frac{\mu}{\rho}\right|\right),$$

where ω is the fractional order and λ are the eigenvalues of the saddle-focus equilibrium point of index 2 in the fractional-order STF system (31). This theorem serves as a theoretical basis for assessing whether the chosen system parameters can support chaotic dynamics. Additionally, it calculates the fractional order ω to identify the range of instability dynamics that trigger chaos.

The following theorem introduces the concept of a $critical\ effective\ dimension\ \Sigma_{cr}$, defined as the maximum total order for which the system does not exhibit chaos. In our analysis, we use this theorem to determine whether the total fractional order enables the onset of chaos.

Theorem 5.2. (Grigorenko and Grigorenko, 2003**)** Let $\Sigma = \omega_1 + \omega_2 + \omega_3$ represent the system's overall effective fractional order. Then, Σ_{cr} is the critical effective dimension, which is the maximum value of Σ where the system remains stable and does not show chaotic behavior for all $\Sigma \leq \Sigma_{\mathrm{cr}}$. That is, the system cannot produce chaotic dynamics if $\Sigma \leq \Sigma_{\mathrm{cr}}$.

In this paper, Theorems 5.1 and 5.2 are purely theoretical and based on previous literature. Our original contribution lies in applying these theorems to the fractional-order STF system (31), validating chaos through numerical simulations that include phase portraits and Lyapunov exponents.

To analyze numerically, the parameter values $r_1 = 1,\ r_2 = 0.1,\ k = 6.2$, and $c = -2$ are considered for the fractional-order STF system (31). Under these parameters, the system has six equilibrium points given by $E_{1,2} = (0, \pm 2, 0), E_{3,4} = (\pm 0.9253, 0.3279, \pm 1.4574)$ and $E_{5,6} = (\pm 0.9423, -0.3175, \pm 1.4371)$. Table 1 summarizes the stability investigation into these equilibrium points.

Table 1: Equilibrium points and their stabilities.

Equilibrium points	**Eigenvalues**	**Nature**
$E_1 = (0, -2, 0)$	$-12, -3.9410, 9.5485$	Unstable Saddle point
$E_2 = (0,2,0)$	$12, 3.9112, -9.5187$	Unstable Saddle point
$E_3 = (-0.9253, 0.3279, -1.4574)$	$1.7636, -0.3578 \pm 9.0540i$	Unstable Saddle-focus point
$E_4 = (0.9253, 03279, 1.4574)$	$1.7636, -0.3578 \pm 9.0540i$	Unstable Saddle-focus point
$E_5 = (0.9423, -0.3175, -1.4371)$	$-1.7175, 0.3514 \pm 9.1832i$	Unstable Saddle-focus point
$E_6 = (-0.9423, -0.3175, 1.4371)$	$-1.7175, 0.3514 \pm 9.1832i$	Unstable Saddle-focus point

The points $E_{1,2}$ are unstable saddle points since they possess two real eigenvalues, one or more of which is positive. While these points indicate instability, they do not contribute to the creation of a scroll. The other points, E_3 to E_6, are unstable saddle-focus points since they possess both nonzero real parts and complex eigenvalues. $E_{3,4}$ are of index 1 and connect

scrolls without producing new ones, as found in (Lu and Chen, 2006). But E_5 and E_6 are of index 2 and are positively involved, with the ability to form scrolls around it. This comparison serves to show a clear difference in the dynamical effect of these equilibrium points in the entire topology of the attractor.

5.1 Critical effective dimension of fractional STF flow

To investigate chaotic behavior in a fractional-order system, it is essential to determine the required critical effective dimension (Grigorenko and Grigorenko, 2003). Based on the theoretical analysis and numerical results presented in Theorem 5.1, the condition necessary for the emergence of chaos is

$$\omega \geq \frac{2}{\pi}\left(\tan^{-1}\left|\frac{9.1832}{0.3514}\right|\right) \approx 0.976.$$

Therefore, each fractional order ω_j must satisfy the $\omega_j \geq 0.976$, in order to maintain the instability of the eigenvalue. By using Theorem 5.2, the hypothesis on the critical effective dimension of the fractional-order STF system (31) is stated as

The fractional-order STF system (31) may have chaotic behavior even if we have the sum of the commensurate fractional orders $\sum = \omega_1 + \omega_2 + \omega_3 = 0.976 + 0.976 + 0.976 = 2.928 \leq 3$, and we have $\sum_{cr} \in (1,3]$.

According to (Tavazoei and Haeri, 2007), a fractional-order chaotic system can only have chaos if it meets a specific chaotification condition. This condition defines the border between stability and instability. Upon fulfillment of the chaotification condition, the system demonstrates chaotic behavior at the specified parameter values. In this particular case, the resulting attractor is typically classified as a self-excited attractor (Leonov and Kuznetsov, 2013). Conversely, if the condition is not met, the system may still exhibit a hidden attractor or coexisting attractor, which does not emerge from the vicinity of any equilibrium point, even though the system appears locally stable in the conventional sense (Jafari and Sprott, 2013).

5.2 Phase portraits

In this subsection, we generate the chaotic phase portraits by using varying values of the fractional order ω to verify the existence of chaos in the parameters we selected in the previous subsection for the system, which were values $r_1 = 1,\ r_2 = 0.1,\ k = 6.2$, and $c = -2$. The fractional-order STF system (31) exhibits chaotic behavior, as illustrated in Figures 8-10.

In Figures 8-10, we plotted numerical solutions for the fractional-order STF system (31) with different fractional orders $\omega = 0.98$, $\omega = 0.99$, and $\omega = 0.999$, respectively. Simulations are based on the same initial conditions $(0.01, 0.01, 0.01)$, evaluated over the time interval $[0, 100]$. In these figures, we displayed the chaotic attractors of system (31), which were obtained using the numerical scheme for the predictor-corrector method. The 3D phase portraits display a two-scroll attractor, indicating trajectories that switch back and forth between two lobes in the phase space in an irregular but bounded manner. As the fractional order escalates from $\omega = 0.98$ to $\omega = 0.999$, the scrolls exhibit greater density and structure, indicative of enhanced folding and stretching, as illustrated in Figures 8a-10a. Further, plots of time series trajectories for $x(t)$, $y(t)$, and $z(t)$ exhibit aperiodic, bounded oscillations, consistent with chaos over the time interval $[0, 100]$, but without any evident periodicity as presented in Figures 8(b)-10(b). The signals in Figure 10 are slightly more irregular and compressed, which suggests enhanced sensitivity and complexity in a higher fractional order. Additionally, Figures 8(c-e) through 10(c-e) illustrate that the 2D projections onto the $xy, xz,$ and yz -planes corroborate these findings. In particular, the structure of the two scrolls is visible, with tighter loops and more intricate layering in Figure 10 compared to Figures 8 and 9. This research suggests that elevating the fractional order towards 1 results in enhanced dynamical behavior and complexity. The data indicate that the system consistently exhibits a chaotic two-scroll attractor at all fractional orders, with geometric complexity and trajectory density escalating as ω approaches 1.

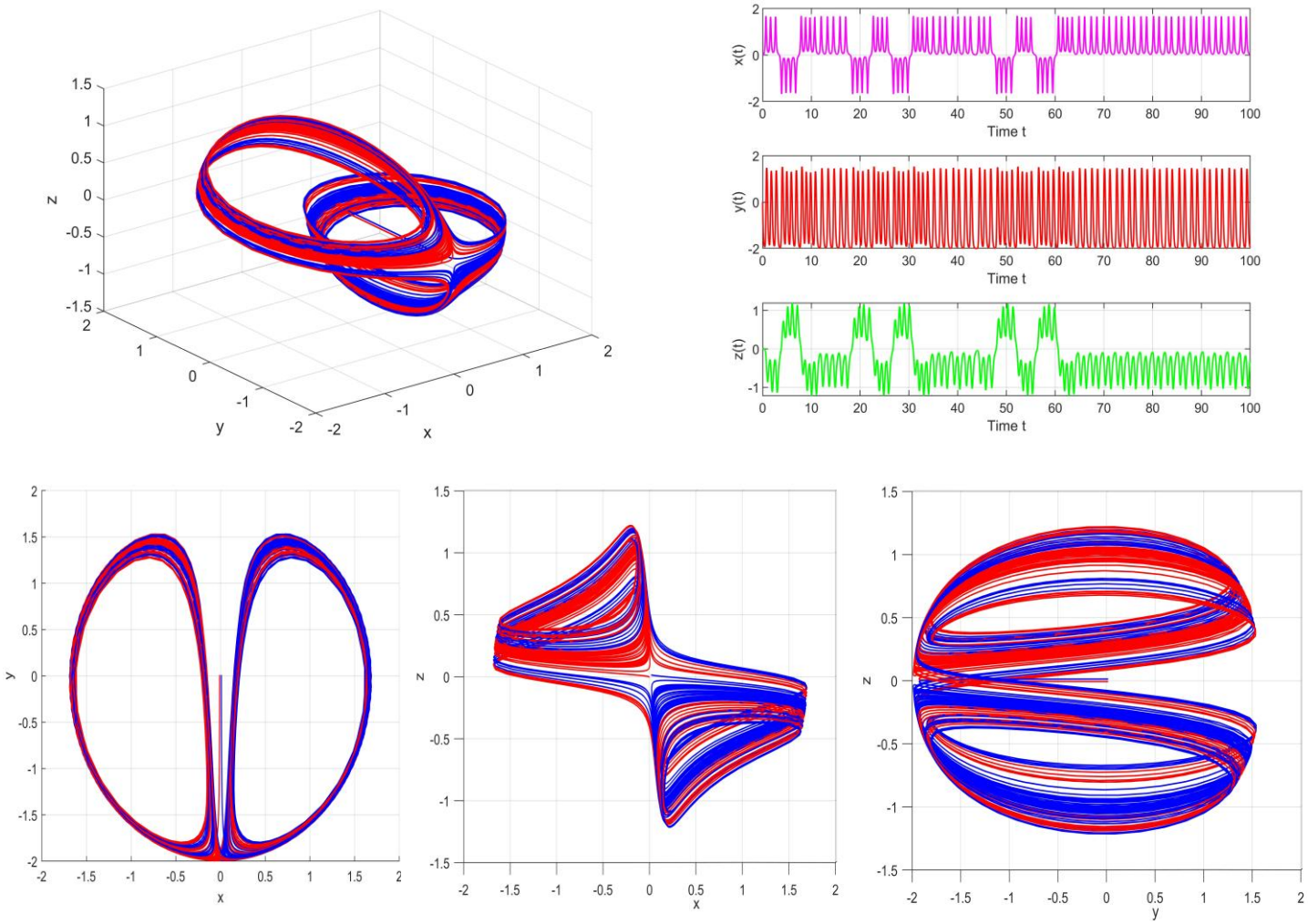

(c) (d) (e)

Figure 8: The phase space diagram and the corresponding time series of the fractional-order STF system (31) of order $\omega = 0.98$. (a) The 3D phase portrait exists in the xyz-space. (b) Trajectories of $x(t), y(t)$ and $z(t)$ over time. (c) Two-dimensional projection across the xy-plane. (d) Two-dimensional projection across the xz-plane. (e) Two-dimensional projection across the yz-plan

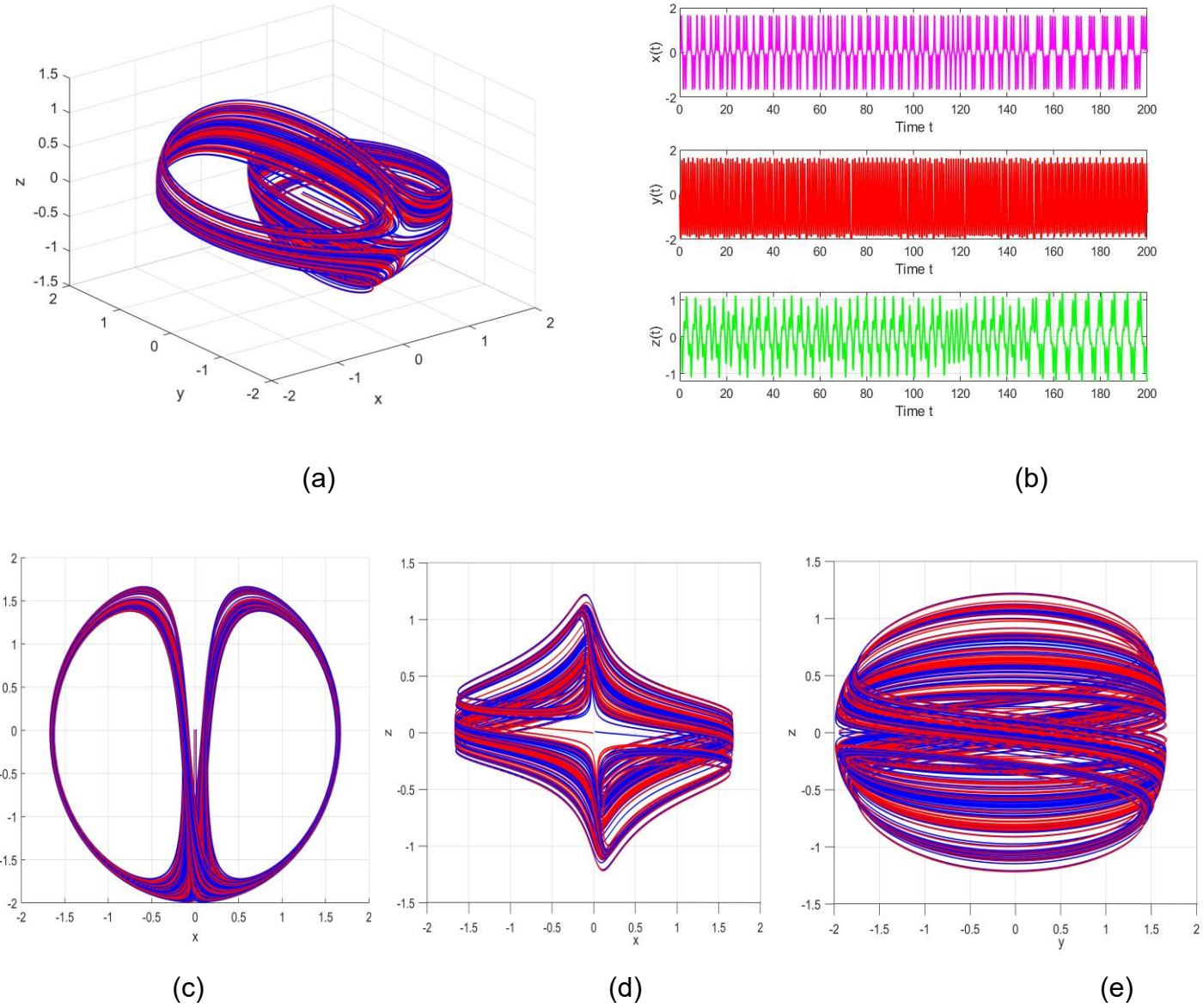

Figure 9: The phase space diagram and the corresponding time series of the fractional-order STF system (31) of order $\omega = 0.99$. (a) The 3D phase portrait exists in the xyz-space. (b) Trajectories of $x(t), y(t)$ and $z(t)$ over time. (c) Two-dimensional projection across the xy-plane. (d) Two-dimensional projection across the xz-plane. (e) Two-dimensional projection across the yz-plane.

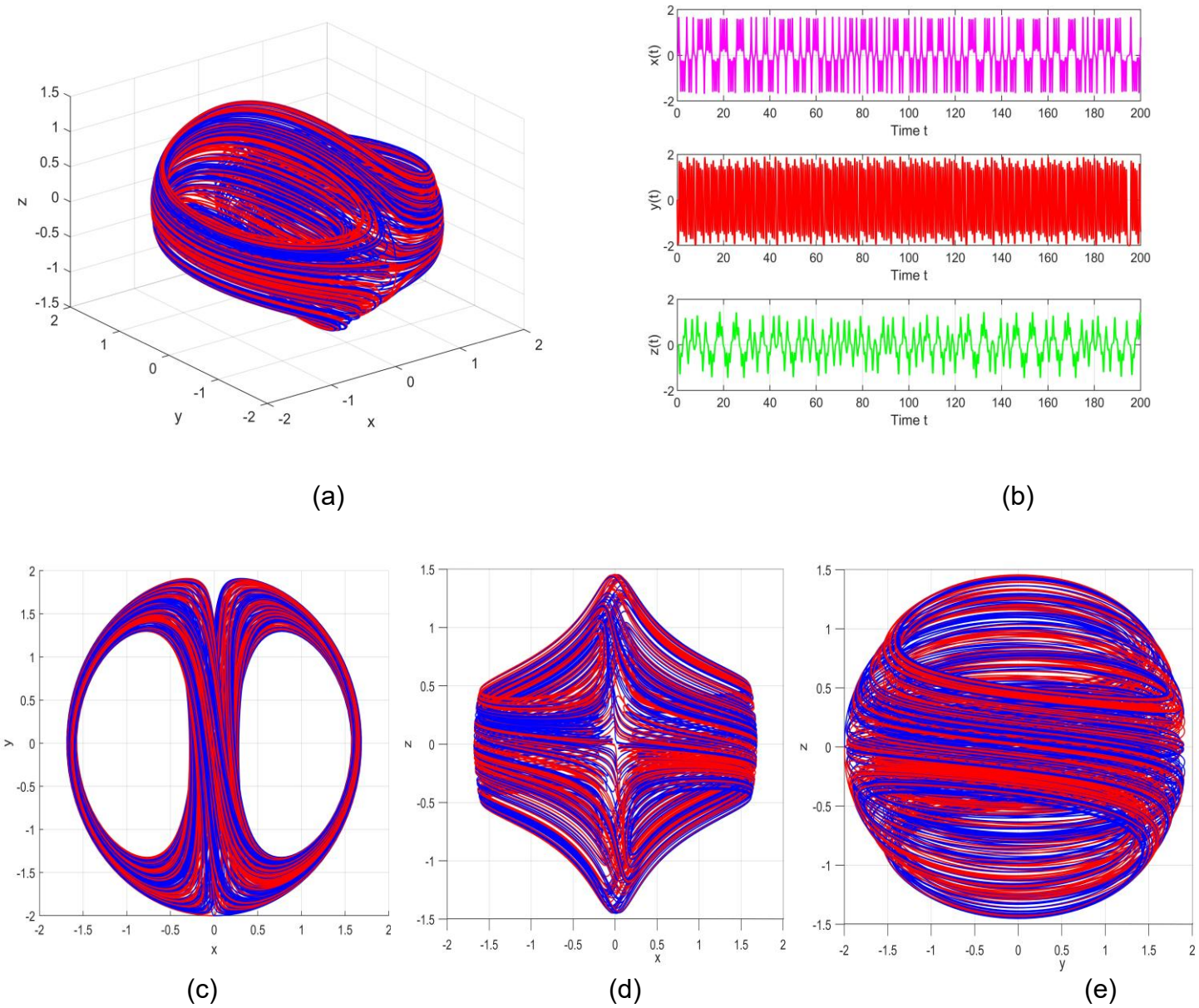

Figure 10: The phase space diagram and the corresponding time series of the fractional-order STF system (31) of order $\omega = 0.999$. (a) The 3D phase portrait exists in the xyz-space. (b) Trajectories of $x(t), y(t)$ and $z(t)$ over time. (c) Two-dimensional projection across the xy-plane. (d) Two-dimensional projection across the xz-plane. (e) Two-dimensional projection across the yz-plane.

5.3 Determining chaos using the Lyapunov exponents

In this subsection, the Lyapunov exponents are applied to the fractional-order STF system (31) using the Danca algorithm (Danca and Kuznetsov, 2018) to determine its chaotic behavior. These exponents provide a fundamental tool for identifying chaos, particularly when at least one of them is positive, signifying that the system is entirely

unpredictable. For all numerical simulations, we fixed the step size of h=0.006. The dynamic behavior of the system includes calculating the three Lyapunov exponents, namely $LE1$, $LE2$, and $LE3$, as shown in Figure 11. The Lyapunov exponents are determined for the time t from 0 to 1000 with a fractional order of $\omega = 0.99$, yielding values of $(LE1, LE2, LE3) = (0.5774, -0.0030, -0.8757)$, given in Table 2. The positive outcome of $LE1$ validates the chaotic behavior of the fractional-order STF system (31). Moreover, at all lines, the sum of the Lyapunov exponents is negative (the fractional-order STF loses energy over time). This result signifies that the solutions of the fractional-order system exhibit chaotic behavior.

Table 2: Lyapunov Exponents at selected time steps.

Time	LE1	LE2	LE3
50	0.6002	-0.0299	-0.9090
100	0.6336	-0.0330	-0.9330
150	0.6181	-0.0255	-0.9052
200	0.6030	-0.0170	-0.8985
250	0.5995	-0.0114	-0.9080
300	0.5840	-0.0044	-0.8916
350	0.5862	-0.0037	-0.8990
400	0.5905	-0.0080	-0.8998
450	0.5910	-0.0016	-0.9043
500	0.5941	-0.0057	-0.9005
550	0.5967	-0.0032	-0.8992
600	0.5938	-0.0004	-0.8934
650	0.5911	-0.0023	-0.8962
700	0.5839	-0.0027	-0.8863
750	0.5828	-0.0051	-0.8820
800	0.5773	-0.0024	-0.8788
850	0.5705	-0.0001	-0.8727
900	0.5748	-0.0006	-0.8769
950	0.5767	-0.0030	-0.8760
1000	0.5774	-0.0030	-0.8757

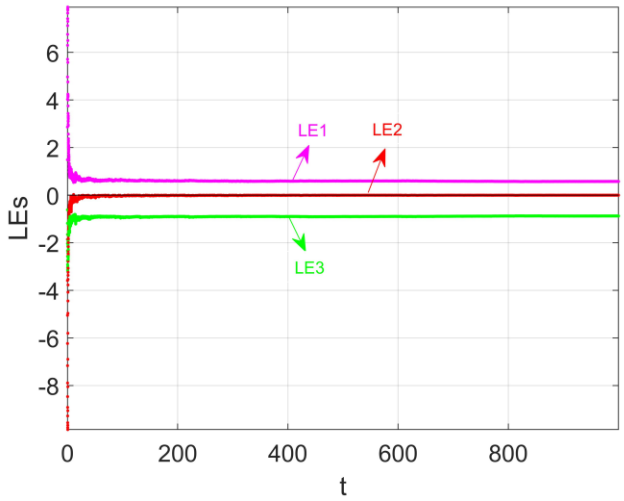

Figure 11: Lyapunov exponents with respect to time.

The Lyapunov exponents are significantly influenced by the system parameters $r_1 = 1$, $r_2 = 0.1$, $k = 6.2$, and $c = -2$, with initial values ($0.01,0.01,0.01$), where ω is in the interval $(0.9,1]$. In Figure 12, the greatest Lyapunov exponent is positive throughout a spectrum of ω, confirming the persistence of chaos across varying orders. This chart demonstrates the significant role of the fractional derivative in modulating system stability and complexity. The corresponding numerical values for the Lyapunov exponents under varying values of ω are shown in Table 3.

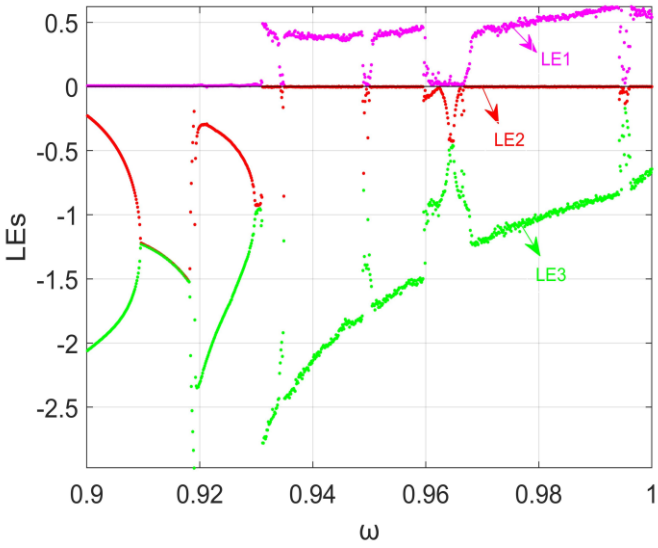

Figure 12: Lyapunov exponents with order ω.

Table 3: Lyapunov exponents with varying values of ω.

ω	LE1	LE2	LE3
0.98	0.5343	-0.0025	-1.0429
0.985	0.5455	-0.0005	-0.9389
0.99	0.5774	-0.0030	-0.8757
0.995	0.2035	-0.0617	-0.3978
0.999	0.5701	-0.0004	-0.7017
1	0.5481	-0.0024	-0.6362

Furthermore, to explore the impact of the control parameter k, we fix other parameters at the same previous values: $r_1 = 1$, $r_2 = 0.1$, and $c = -2$, with corresponding initial values $(0.01, 0.01, 0.01)$, and $\omega = 0.99$. Figure 13 shows the variation of $LE1$, $LE2$, and $LE3$ with respect to k. The figure indicates that chaos emerges for values of k such that $4.8 \lesssim k \lesssim 10.5$, during which $LE1$ becomes positive. These transitions indicate a bifurcation in the system. $LE2$ remains near zero, and $LE3$ stays negative, consistent with chaotic dynamics characterized by divergence in at least one direction. These findings underscore the importance of the parameter k in influencing the stability and chaotic behavior of the fractional-

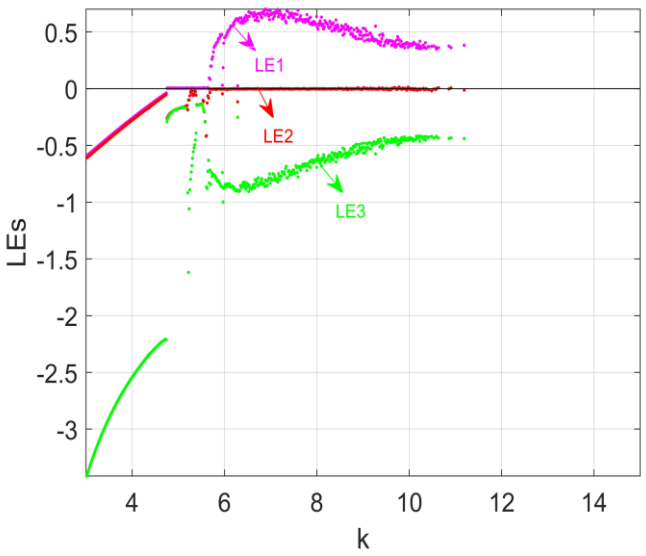

Figure 13: Lyapunov exponents with control parameter k.

6 Conclusion

In this paper, the modified stretch-twist-fold (STF) flow system (31) with fractional order was investigated. The study started with finding the system's equilibrium points. The stability and the Hopf bifurcation occurrence at all equilibrium points were investigated using a numerical predictor-corrector technique by the proper choice of parameter values, as shown in Figures 2–7. In addition, we selected suitable parameters that met the conditions for fractional order and effective dimension to investigate the potential for chaotic behavior. Phase portraits of the system for different fractional orders (Figures 8–10) and the largest Lyapunov exponents (Figure 11, Table 2) were utilized to illustrate the dynamics of the system. Figure 12 and Table 3 further demonstrate the results by identifying the occurrence of chaos with varying fractional order. Overall, the results reveal that the control parameters and the fractional order considerably affect the dynamic behavior of the system.

References

Abdelouahab, M.-S., et al. (2012). "Hopf bifurcation and chaos in fractional-order modified hybrid optical system." Nonlinear Dynamics **69**: 275-284.

Abualhomos, M., et al. (2023). "Bifurcation, Hidden Chaos, Entropy and Control in Hénon-Based Fractional Memristor Map with Commensurate and Incommensurate Orders." Mathematics **11**(19): 4166.

Ahmed, E., et al. (2007). "Equilibrium points, stability and numerical solutions of fractional-order predator–prey and rabies models." Journal of Mathematical Analysis and Applications **325**(1): 542-553.

Asgari-Targhi, M. and M. A. Berger (2009). "Writhe in the stretch-twist-fold dynamo." Geophysical and Astrophysical Fluid Dynamics **103**(1): 69-87.

Azam, A., et al. (2017). "Chaotic behavior of modified stretch-twist-fold (STF) flow with fractal property." Nonlinear Dynamics **90**(1): 1-12.

Bajer, K. (1989). Flow kinematics and magnetic equilibria, University of Cambridge.

Bandyopadhyay, B. and S. Kamal (2015). "Stabilization and control of fractional order systems: a sliding mode approach."

Bao, J. and Q. Yang (2010). "Complex dynamics in the stretch-twist-fold flow." Nonlinear Dynamics **61**: 773-781.

Bao, J. and Q. Yang (2014). "Bifurcation analysis of the generalized stretch-twist-fold flow." Applied Mathematics and Computation **229**: 16-26.

Bao, J. and Q. Yang (2014). "Darboux integrability of the stretch-twist-fold flow." Nonlinear Dynamics **76**: 797-807.

Bhalekar, S. and D. Gupta (2022). "Stability and bifurcation analysis of a fractional order delay differential equation involving cubic nonlinearity." Chaos, Solitons & Fractals **162**: 112483.

Cafagna, D. and G. Grassi (2008). "Bifurcation and chaos in the fractional-order Chen system via a time-domain approach." International Journal of Bifurcation and Chaos **18**(07): 1845-1863.

Chettouh, B. and T. Menacer (2024). "Effect of fractional order on the stability and the localisation of the critical Hopf bifurcation value in a fractional chaotic system." International Journal of Dynamics and Control **12**(6): 1707-1716.

Childress, S. and A. D. Gilbert (2008). Stretch, twist, fold: the fast dynamo, Springer Science & Business Media.

Danca, M.-F. (2023). "Symmetry-breaking and bifurcation diagrams of fractional-order maps." Communications in Nonlinear Science and Numerical Simulation **116**: 106760.

Danca, M.-F. and N. Kuznetsov (2018). "Matlab code for Lyapunov exponents of fractional-order systems." International Journal of Bifurcation and Chaos **28**(05): 1850067.

Das, S. (2011). Introduction to fractional calculus. Functional fractional calculus, Springer**:** 1-50.

Deshpande, A. S., et al. (2017). "On Hopf bifurcation in fractional dynamical systems." Chaos, Solitons & Fractals **98**: 189-198.

Diethelm, K. and N. Ford (2010). "The analysis of fractional differential equations." Lecture notes in mathematics **2004**.

Diethelm, K., et al. (2002). "A predictor-corrector approach for the numerical solution of fractional differential equations." Nonlinear Dynamics **29**: 3-22.

Edelman, M., et al. (2023). "Bifurcations and transition to chaos in generalized fractional maps of the orders 0< α< 1." Chaos: An Interdisciplinary Journal of Nonlinear Science **33**(6).

El-Saka, H., et al. (2009). "On stability, persistence, and Hopf bifurcation in fractional order dynamical systems." Nonlinear Dynamics **56**: 121-126.

Ghaziani, R. K., et al. (2016). "Stability and dynamics of a fractional order Leslie–Gower prey–predator model." Applied Mathematical Modelling **40**(3): 2075-2086.

Grigorenko, I. and E. Grigorenko (2003). "Chaotic dynamics of the fractional Lorenz system." Physical review letters **91**(3): 034101.

Hu, W., et al. (2017). "Hopf bifurcation and chaos in a fractional order delayed memristor-based chaotic circuit system." Optik **130**: 189-200.

Hussein, N. H. and A. I. Amen (2019). "Zero-Hopf bifurcation in the generalized stretch-twist-fold flow." Sultan Qaboos University Journal for Science [SQUJS] **24**(2): 122-128.

Jafari, S. and J. Sprott (2013). "Simple chaotic flows with a line equilibrium." Chaos, Solitons & Fractals **57**: 79-84.

Jafari, S., et al. (2016). "A simple chaotic flow with a plane of equilibria." International Journal of Bifurcation and Chaos **26**(06): 1650098.

Ji, Y., et al. (2018). "Bifurcation and chaos of a new discrete fractional-order logistic map." Communications in Nonlinear Science and Numerical Simulation **57**: 352-358.

Kaslik, E. and S. Sivasundaram (2012). "Nonlinear dynamics and chaos in fractional-order neural networks." Neural networks **32**: 245-256.

Kiani-B, A., et al. (2009). "A chaotic secure communication scheme using fractional chaotic systems based on an extended fractional Kalman filter." Communications in Nonlinear Science and Numerical Simulation **14**(3): 863-879.

Kilbas, A. A., et al. (2006). Theory and applications of fractional differential equations, elsevier.

Leonov, G. A. and N. V. Kuznetsov (2013). "Hidden attractors in dynamical systems. From hidden oscillations in Hilbert–Kolmogorov, Aizerman, and Kalman problems to hidden chaotic attractor in Chua circuits." International Journal of Bifurcation and Chaos **23**(01): 1330002.

Leung, A. Y., et al. (2014). "Periodic bifurcation of Duffing-van der Pol oscillators having fractional derivatives and time delay." Communications in Nonlinear Science and Numerical Simulation **19**(4): 1142-1155.

Li, X. and R. Wu (2014). "Hopf bifurcation analysis of a new commensurate fractional-order hyperchaotic system." Nonlinear Dynamics **78**: 279-288.

Liu, X. and L. Hong (2013). "Chaos and adaptive synchronizations in fractional-order systems." International Journal of Bifurcation and Chaos **23**(11): 1350175.

Liu, X., et al. (2016). "Global bifurcations in fractional-order chaotic systems with an extended generalized cell mapping method." Chaos: An Interdisciplinary Journal of Nonlinear Science **26**(8).

Lu, J. G. and G. Chen (2006). "A note on the fractional-order Chen system." Chaos, Solitons & Fractals **27**(3): 685-688.

Lyubomudrov, O., et al. (2003). "Pseudochaotic systems and their fractional kinetics." International Journal of Modern Physics B **17**(22n24): 4149-4167.

Machado, J. T. and A. M. Galhano (2018). "A fractional calculus perspective of distributed propeller design." Communications in Nonlinear Science and Numerical Simulation **55**: 174-182.

Maciejewski, A. J. and M. Przybylska (2020). "Integrability analysis of the stretch–twist–fold flow." Journal of Nonlinear Science **30**(4): 1607-1649.

Matignon, D. (1996). Stability results for fractional differential equations with applications to control processing. Computational engineering in systems applications, Lille, France.

Moffatt, H. (1989). "Stretch, twist and fold." Nature **341**(6240): 285-286.

Osman, S. and T. Langlands (2022). "Numerical investigation of two models of nonlinear fractional reaction subdiffusion equations." Fractional Calculus and Applied Analysis **25**(6): 2166-2192.

Podlubny, I. (1998). Fractional differential equations: an introduction to fractional derivatives, fractional differential equations, to methods of their solution and some of their applications, elsevier.

Poincaré, H. (1893). Les méthodes nouvelles de la mécanique céleste, Gauthier-Villars et fils, imprimeurs-libraires.

Sheu, L. J., et al. (2010). "A two-channel secure communication using fractional chaotic systems." World Academy of Science, Engineering and Technology **65**: 1057-1061.

Sprott, J. C. (2011). "A proposed standard for the publication of new chaotic systems." International Journal of Bifurcation and Chaos **21**(09): 2391-2394.

Suryanto, A., et al. (2025). "Bifurcation Analysis and Chaos Control of a Discrete–Time Fractional Order Predator-Prey Model with Holling Type II Functional Response and Harvesting." CHAOS Theory and Applications **7**(1): 87-98.

Tavazoei, M. S. and M. Haeri (2007). "A necessary condition for double scroll attractor existence in fractional-order systems." Physics Letters A **367**(1-2): 102-113.

Tavazoei, M. S. and M. Haeri (2008). "Limitations of frequency domain approximation for detecting chaos in fractional order systems." Nonlinear Analysis: Theory, Methods & Applications **69**(4): 1299-1320.

Tavazoei, M. S. and M. Haeri (2009). "Describing function based methods for predicting chaos in a class of fractional order differential equations." Nonlinear Dynamics **57**(3): 363-373.

Tenreiro Machado, J., et al. (2015). "Fractional state space analysis of economic systems." Entropy **17**(8): 5402-5421.

Uddin, M. J. (2022). "Analysis of bifurcation and chaos to fractional order Brusselator model." Journal of Applied Mathematics and Computation **6**(3).

Vainshtein, S. I., et al. (1997). "Stretch-twist-fold and ABC nonlinear dynamos: restricted chaos." Physical Review E **56**(2): 1605.

Vainshtein, S. I., et al. (1996). "Fractal properties of the stretch-twist-fold magnetic dynamo." Physical Review E **53**(5): 4729.

Vainshtein, S. I. and Y. B. Zel'dovich (1972). "Origin of magnetic fields in astrophysics (turbulent "dynamo" mechanisms)." Soviet Physics Uspekhi **15**(2): 159-172.

Wang, C., et al. (2023). "Bifurcation and Chaotic Behavior of Duffing System with Fractional-Order Derivative and Time Delay." Fractal and Fractional **7**(8): 638.

Xiao, M. and W. X. Zheng (2012). Nonlinear dynamics and limit cycle bifurcation of a fractional-order three-node recurrent neural network. 2012 IEEE International Symposium on Circuits and Systems (ISCAS), IEEE.

Yue, B. and M. Aqeel (2013). "Chaotification in the stretch-twist-fold (STF) flow." Chinese Science Bulletin **58**: 1655-1662.

Zhi, Y., et al. (2022). "Computational methods for nonlinear analysis of Hopf bifurcations in power system models." Electric Power Systems Research **212**: 108574.